J. Biomed. Eng. Res : 177-186, 2010

# In vivo Evaluation of Flow Estimation Methods for 3D Color Doppler Imaging

Yangmo Yoo

*Department of Electronic Engineering and Interdisciplinary Program of Integrated Biotechnology*
*(Received January 13, 2010. Accepted April 26, 2010)*

Abstract

In 3D ultrasound color Doppler imaging (CDI), 8-16 pulse transmissions (ensembles) per each scanline are used for effective clutter rejection and flow estimation, but it yields a low volume acquisition rate. In this paper, we have evaluated three flow estimation methods: autoregression (AR), eigendecomposition (ED), and autocorrelation combined with adaptive clutter rejection (AC-ACR) for a small ensemble size (E=4). The performance of AR, ED and AC-ACR methods was compared using 2D and 3D *in vivo* data acquired under different clutter conditions (common carotid artery, kidney and liver). To evaluate the effectiveness of three methods, receiver operating characteristic (ROC) curves were generated. For 2D kidney *in vivo* data, the AC-ACR method outperforms the AR and ED methods in terms of the area under the ROC curve (AUC) (0.852 vs. 0.793 and 0.813, respectively). Similarly, the AC-ACR method shows higher AUC values for 2D liver *in vivo* data compared to the AR and ED methods (0.855 vs. 0.807 and 0.823, respectively). For the common carotid artery data, the AR provides higher AUC values, but it suffers from biased estimates. For 3D *in vivo* data acquired from a kidney transplant patient, the AC-ACR with E=4 provides an AUC value of 0.799. These *in vivo* experiment results indicate that the AC-ACR method can provide more robust flow estimates compared to the AR and ED methods with a small ensemble size.

Key words : Ultrasound imaging; 3D color Doppler imaging; autoregression, eigendecomposition, autocorrelation, adaptive clutter rejection

## I. INTRODUCTION

3D color Doppler imaging (CDI) combines the directional flow information of 2D CDI and the advantages of 3D ultrasound[1]. It is useful for noninvasively evaluating hemodynamic changes with simultaneous visualization of surrounding tissues, e.g., assessment of mitral regurgitation [2], fetal congenital heart defects[3] and stroke volume measurement[4]. Compared to 3D B-mode ultrasound imaging where a single pulse transmission is needed for each scanline, 3D CDI has a lower volume acquisition rate because an ensemble of pulse transmissions (typically 8 to 16) is required for each scanline to obtain flow information via a commonly-used autocorrelation (AC) method[5,6]. This relatively-large ensemble size is necessary to adequately suppress the strong backscattering from slow-moving tissues and stationary echoes (i.e., clutter), which obscures the weak scattering from blood flow. The low volume acquisition rate also decreases the temporal resolution of 3D CDI, which could lead to inaccurate in flow quantification[7,8] and cause flash artifacts due to patient and/or probe motion.

One approach to improve the volume rate is to decrease the ensemble size for flow estimation. However, it is challenging to design an appropriate clutter filter with small ensemble sizes. For example, since a finite impulse response (FIR) filter reduces the number of data samples available for flow estimation, it cannot be used for clutter rejection with small ensemble sizes (e.g., 4 and 6). On the other hand, projection-initialized infinite impulse response (PI-IIR) and polynomial regression (PR) filters do not reduce the number of data samples for flow estimation, but they may introduce a bias on flow estimation due to their time-varying impulse response[9-11]. To improve clutter rejection in AC, several adaptive clutter suppression techniques, such as eigenvector filtering and adaptive clutter rejection, have been proposed [9,12-13]. Eigenvector filtering can theoretically provide the maximum clutter suppression due to its best mean square approximation of the clutter. However, it could remove the

**Corresponding Author** : Yang No Yoo
Department of Electronic Engineering
1 Shinsu-dong, Mapo-gu, Seoul 121-742, Korea
Tel : +82-2-705-4731 / Fax : +82-2-707-3008
Email : ymyoo@sogang.ac.kr
Revised and re-submitted to the Journal of Biomedical Engineering Research in April 2010
Submitted to the Journal of Biomedical Engineering Research in December 2009

flow signal close to the clutter frequency due to a limitation in accurately determining the clutter subspace dimension[13].

Alternatively, a flow estimation algorithm that is capable of directly extracting the flow signals without clutter rejection can be utilized. Several new flow estimation techniques, such as autoregression (AR) and eigendecomposition (ED), have been proposed to separate clutter and flow without applying a highpass clutter filter[14-19]. From previous studies, the AR and ED methods adequately suppress clutter, but quantitative evaluations on the robustness of these two methods using small ensemble sizes under realistic *in vivo* conditions for 3D CDI are still lacking.

In this paper, we quantitatively evaluate the sensitivity and specificity of three estimation methods (i.e., AR, ED and AC) under different clutter conditions using 2D and 3D *in vivo* data acquired using a commercial ultrasound machine. To separate flow signals from noise, the local statistics (i.e., standard deviation) of flow estimates and the ratio of singular values were used for the AR and ED estimators, respectively. For the AC method, the adaptive clutter filtering where an optimum filter is selected based on measured clutter characteristics was used.

## II. METHODS

In this section, we introduce three flow estimation methods, i.e., AC-ACR, AR and ED. Also, the experimental setup, including evaluation metric, is presented.

### A. Flow estimation methods

For each temporal sample, the backscattered quadrature-demodulated signal from the $e^{th}$ successive transmitted ultrasound pulse can be expressed by[9]

$$y(e) \approx c(e) + f(e) + n(e) \tag{1}$$

where $c(e)$ and $f(e)$ are the complex baseband signals representing the backscattering from tissues and flow scatterers, respectively, and $n(e)$ is additive noise. The signal in Eq. (1) can be rewritten with a 1D complex column vector as follows:

$$Y = [y(0) \;\; y(1) \;\; \ldots \;\; y(E-1)]^T \tag{2}$$

where $E$ is the ensemble size.

1) Autocorrelation with adaptive clutter rejection (AC-ACR)

With autocorrelation-based estimation, a clutter filter is applied to the complex baseband signal in Eq. (2) to remove the clutter that is typically 40 to 60 dB stronger than the flow signal (i.e., $|c(e)| \gg |f(e)|$), which leads to a bias in flow velocity estimates. In the AC method, an estimate of the first lag of the filtered complex correlation squence, $\Gamma_{yyf}(1)$, is obtained by

$$\Gamma_{yyf}(1) = \frac{1}{E-1} \sum_{m=0}^{E-2} y_f(m) y_f(m+1)^* \tag{3}$$

where $y_f(m)$ is the filtered complex sequence where the clutter has been substantially attenuated and * represents a complex conjugate operation. The mean flow velocity can be calculated by

$$v_f = \frac{c}{4\pi T_{prf} f_0} \tan^{-1}\left[\frac{\mathrm{Im}(\Gamma_{yyf}(1))}{\mathrm{Re}(\Gamma_{yyf}(1))}\right] \tag{4}$$

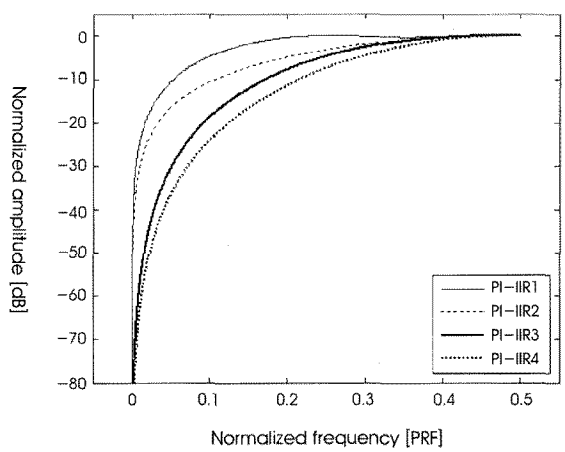


**Fig. 1.** Amplitude response of four different clutter filters using PI-IIR filters for E=4 where the PRF represents the normalized pulse repetition frequency.

where $f_0$ is the center frequency of the transmitted ultrasound beam, c is the sound velocity, and $T_{prf}$ is the pulse repetition interval.

In the present study, the adaptive clutter rejection (ACR) method, in which a suitable clutter filter from the pre-designed filter bank is selected based on clutter power and its instanteneous velocities, is used as part of the AC method (i.e., AC-ACR)[11,19]. Fig. 1 shows the amplitude response of the pre-designed PI-IIR filters for E=4. The more detailed explanation of ACR can be found elsewhere[20].

2) Autoregression (AR) estimation

In the AR estimation, the Doppler signal containing the clutter and flow is represented with the second-order AR model. Unlike AC-ACR, the AR estimation does not require clutter rejection since its two poles are assumed to directly represent the clutter and flow components. The $e^{th}$ complex baseband data in Eq. (2) can be predicted as a linear combination of $p$ previous sequences

$$y(e) = \sum_{n=1}^{p} a_n y(e-n) \tag{5}$$

where $a_n$ is the prediction coefficient for the $n^{th}$ previous sequence.

In the present study, we estimate $a_n$ via the Burg algorithm as used by others[14,15]. For the second-order AR model, two poles are calcuated from two AR parameters (i.e., $a_1$ and $a_2$) by

$$P_{1,2} = \frac{a_1 \pm \sqrt{a_1^2 + 4a_2}}{2} \tag{6}$$

The two velocities correponding to these two poles can be obtained from their phases as follows:

$$v_1 = \frac{c}{4\pi T_{prf} f_0} \tan^{-1}\left[\frac{\mathrm{Im}(P_1)}{\mathrm{Re}(P_1)}\right] \tag{7}$$

$$v_2 = \frac{c}{4\pi T_{prf} f_0} \tan^{-1}\left[\frac{\mathrm{Im}(P_2)}{\mathrm{Re}(P_2)}\right] \tag{8}$$

The absolute value (i.e., a distance from the origin) of the second pole, which is assumed to represent the flow, is used as power. However, this absolute value may not be reliable for removing the biased estimates with a small ensemble size (i.e., E=4). In the present study, we used the standard deviation *(STD)* of flow estimates in a window (e.g., 5 × 5 pixels) in order to remove the estimates that had been biased towards higher velocities due to noise. If the calculated STD is greater than a threshold *(LS)*, the estimated flow velocity, $v_f$, is assigned to be 0. Otherwise, $v_2$ becomes $v_f$.

3) Flow estimation based on eigendecomposition (ED)

In the eigendecomposition-based flow estimation, three components (i.e., clutter, flow and noise) in the complex baseband Doppler data in Eq. (2) are assumed to be statitically independent[10,13]. Thus, the complex signal covariance matrix can be expressed by

$$R_Y = R_{Y_c} + R_{Y_f} + \sigma_n^2 I \tag{9}$$

where $R_{Y_c}$ and $R_{Y_f}$ are the covariance matrix for the clutter and flow, respectively, $\sigma_n^2$ is the noise variance, and $I$ is the identity matrix. In the present study, the modified covariance method was used to estimate $R_Y$ from $Y$ because it can provide more accurate estimates[21]. Using singular-value decomposition (SVD)[22], $R_Y$ can be factorized as follows:

$$R_Y = USV^{\dagger} \tag{10}$$

where $U$ and $V$ are the orthogonal matrices containing singular vectors, $S$ is the diagnonal matrix for singular values, and $^{\dagger}$ is the conjuage transpose operation. In the ED method, the two dominant velocities are calcuated from the phases of the first two singular vectors (i.e., ., $V_1$ and $V_2$) as

$$v_1 = \frac{c}{4\pi T_{prf} f_0} \tan^{-1}\left[\frac{\mathrm{Im}(V_1)}{\mathrm{Re}(V_1)}\right] \tag{11}$$

$$v_2 = \frac{c}{4\pi T_{prf} f_0} \tan^{-1}\left[\frac{\mathrm{Im}(V_2)}{\mathrm{Re}(V_2)}\right] \tag{12}$$

To remove the biased estimates due to noise where there is only tissue, the ratio of the first two singular values on a logarithm scale (i.e., $10\log_{10}[S_2/S_1]$) is compared with a predetermined threshold, $AD$. If the ratio is smaller than $AD$ (i.e., two singular values contain only tissue information), $v_f$ is assigned to be 0 for removing the biased estimates. Otherwise, the velocity from the second singular vector (i.e., $v_2$) becomes $v_f$. It must be noted that the computational complexity of the ED method is much higher than that of the AC-ACR method since it requires a computationally-expensive SVD operation.

**Table 1.** System parameters used in *in vivo* studies.

| Parameters | Values | | | |
|---|---|---|---|---|
| | CCA | Liver | Kidney | 3D |
| Probe | Linear | Convex | Convex | Convex |
| Transmit center frequency [MHz] | 6.5 | 3.5 | 3.5 | 3.5 |
| Pulse repetition frequency [kHz] | 3.5 | 1 | 1 | 1 |
| Ensemble size | 10 | 10 | 10 | 10 |
| Frames | 36 | 36 | 36 | 48 |

### B. Experimental setup

To evaluate the AC-ACR, AR and ED flow estimation methods under different clutter conditions, 2D *in vivo* data were acquired from the common carotid artery (CCA), kidney and liver of five volunteers by a trained sonographer using a commerical ultrasound machine equipped with a programmable back-end system (HiVision 5500, Hitachi Medical Systems America, Twinsburg, OH, USA). As listed in Table 1, 36 consecutive frames of in-phase and quadrature data with E=10 were captured after beamforming and quadrature demodulation, but before clutter filtering and other color Doppler processing. The acquired data were processed off-line using MATLAB (The Mathworks Inc., Natick, MA, USA). A 6.5-MHz linear array transducer was used for acquiring CCA data, while a 3.5-MHz convex array transducer was used for kidney and liver data. To compare three estimators with E=4, only the first four data in an ensemble of 10 were used, and then the obtained results were compared with those from the standard AC method with E=10. Fig. 2 shows the amplitude responses of six clutter filters designed for the AC-ACR with E=10. Also, a 3D *in vivo* kidney data set with 48 frames was acquired from a kidney transplant patient scheduled for a renal transplant biopsy procedure.

### C. Evaluation criteria

The flow signal-to-clutter ratio (SCR) that was used previously[10,11] is difficult to utilize in case of AR estimation with a small ensemble size, since the separation of noise from flow is challenging based on the power estimated from the AR poles. Therefore, a mask for the flow area was generated using the AC-ACR method with E=10. Pixels estimated to be flow by each estimator with E=4 and located within the flow mask were counted as true positive *(TP)*, whereas those flow pixels located outside the flow mask were counted as false positive *(FP)*. Similarly, true negative *(TN)* and false negative *(FN)* were generated. Fig. 3(a) and 3(b) show the pre-scan-converted CCA color Doppler images with velocity and power estimates, respectively, from AC-ACR with E=10. A flow mask from the power estimate (Fig. 3(b)) is shown in Fig. 3(c). The power estimate was used in determining the flow mask due to their higher sensitivity to flow compared to the velocity estimate. From the four groups (i.e., *TP*, *FP*, *TN* and *FN*), the sensitivity and specificity of each estimator are computed by

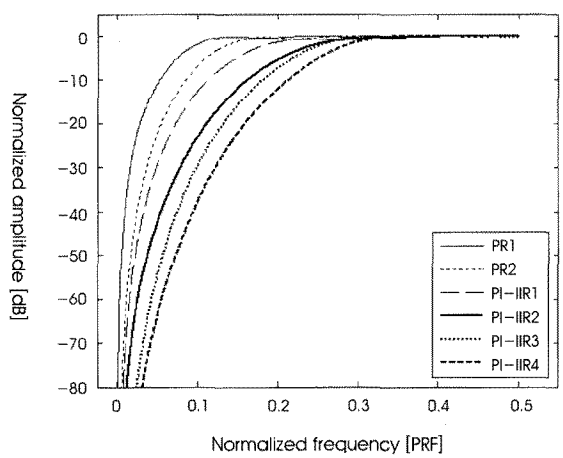


**Fig. 2.** Amplitude response of six polynomial regression (PR) and PI-IIR filters for E=10.

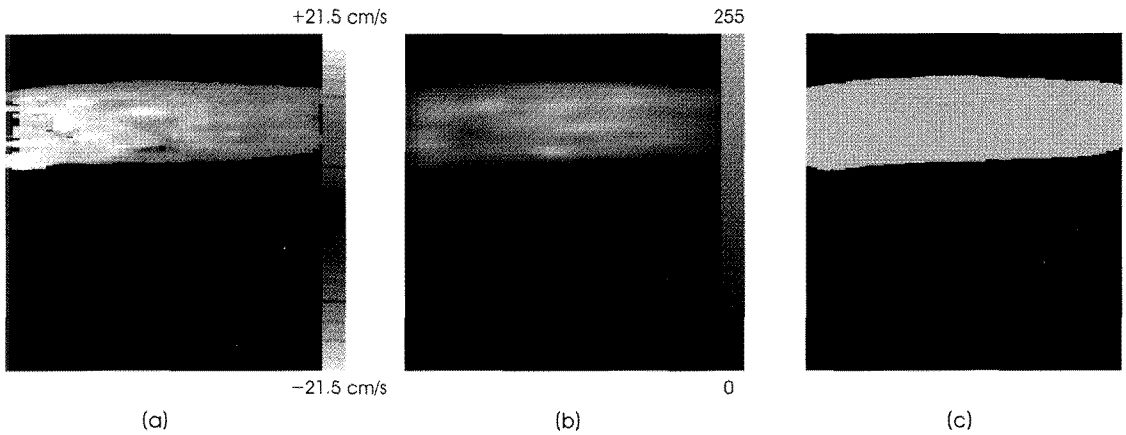


**Fig. 3.** Pre-scan-converted color Doppler image with (a) velocity estimates and (b) power estimates, and (c) flow mask.

$$Sensitivity = \frac{TP}{TP+FN} \tag{13}$$

$$Specificity = \frac{TN}{TN+FP} \tag{14}$$

We performed an ROC analysis where the sensitivity and specificity of the ED estimator were investigated by adjusting the power threshold (i.e., AD=-10, -20, -30, -40, -50 and -60 dB). For the AR estimator, we computed the standard deviation *(STD)* of flow estimates with 3 different window sizes (i.e., 3×3, 5×5 and 7×7 pixels) and used 6 different LS threshold values (i.e., 0.15, 0.20, 0.25, 0.30, 0.35 and 0.40 PRF) to separate flow from noise. For the AC-ACR estimator, we adjusted the power gain *(PG)* to measure its sensitivity and specificity (i.e., *PG*=1.5, 2.5, 3.5, 4.5, 5.5, and 6.5). The area under the ROC curve (AUC) for each estimator was computed. The obtained AUC values from the AC-ACR, AR and ED estimators were analyzed by a two-sided ANOVA. In the present study, a $p$-value less than 0.05 is considered as statistically significant.

## Ⅲ. RESULTS & DISCUSSION

### A. 2D *in vivo* data

Fig. 4 shows the color Doppler images with velocity estimates obtained from the CCA of Subject 1 for E=4 by applying the AR, ED and AC-ACR methods where Fig. 4(a) shows the reference image generated by the AC-ACR method with E=10. For the AR method, the best result was obtained with *LS*=0.3 PRF and a window size of 5×5 pixels. Similarly, an optimal value for *AD* and *PG* was determined to be -50 dB and 3.5 for the ED and AC-ACR methods, respectively. As shown in Fig. 4, the three flow estimation methods show comparable results upon visual assessment.

The ROC curves for the AR, ED and AC-ACR estimators, where the FP fraction (1-specficity) and the TP fraction (sensitivity) are plotted, were generated by adjusting

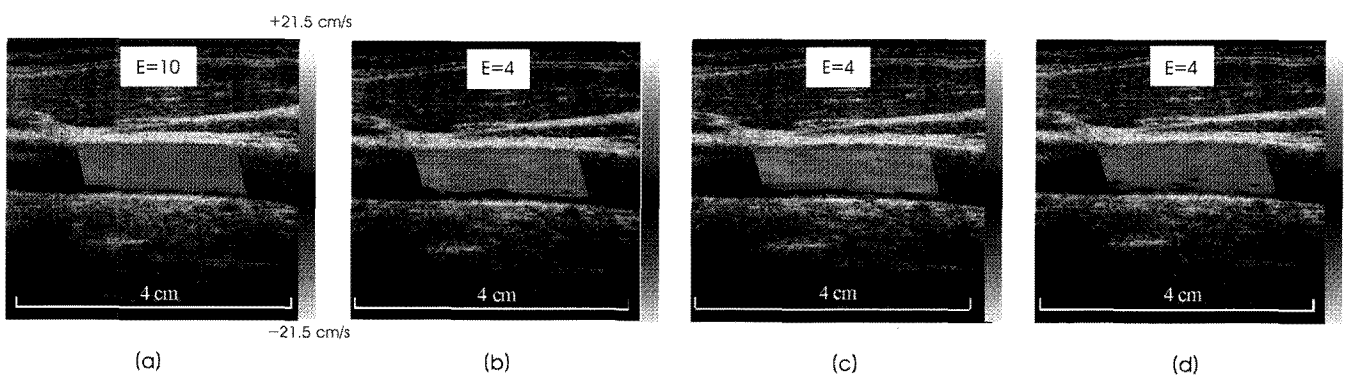


**Fig. 4.** Color Doppler images obtained from the common carotid artery (CCA) of the Subject 1 by applying (a) autocorrelation (AC) with the ACR (AC-ACR) when E=10 as the reference, (b) autoregression (AR), (c) eigendecomposition (ED), and (d) AC-ACR methods. E represents the ensemble size.

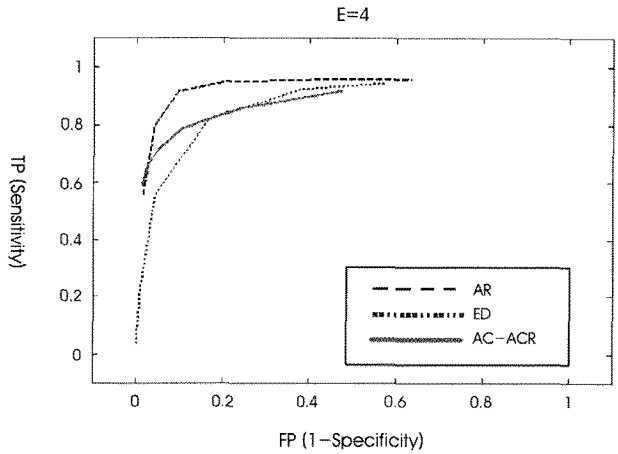


**Fig. 5.** Receiver operating characteristic (ROC) curves when applying the AR, ED and AC-ACR estimators into the 2D CCA data for E=4. The dashed black, dotted blue and solid red lines represent the fitted lines for the AR, ED and AC-ACR estimators, respectively.

parameters (i.e., *LS, AD* and *PG*) as shown in Fig. 5. The AR estimator exhibits the higher TP values, particularly at lower FP values than the ED and AC-ACR estimators for E=4.

The overall performance of the three estimators is quantified by measuring the area under the ROC curve (AUC) for all five subjects. The computed AUC values are tabulated in Table 2. As listed in Table 2, in case of the CCA data, the AR estimator provides the higher AUC value compared to the ED and AC-ACR estimators (e.g., 0.931 vs. 0.882 and 0.895, respectively). However, we have found that the AR estimator suffers from the outliers that occur during systolic phase because the true flow estimates are misinterpreted as biased estimates.

Compared to the CCA data, the kidney and liver data typically have lower SNRs and flow signal strengths due to longer penetration depth, which make velocity estimation challenging. Fig. 6 shows the kidney color Doppler images when using *LS*=0.3 PRF and a window size of 3×3 pixels,

**Table 2.** Area under receiver operating characteristic (ROC) curve (AUC). When E=10, the AUC is 1.

| Data | Subjects | E=4 | | |
|---|---|---|---|---|
| | | AR | ED | AC−ACR |
| CCA | 1 | 0.938 | 0.882 | 0.893 |
| | 2 | 0.920 | 0.875 | 0.897 |
| | 3 | 0.944 | 0.904 | 0.903 |
| | 4 | 0.922 | 0.877 | 0.887 |
| | 5 | 0.933 | 0.873 | 0.894 |
| | Mean | 0.931 | 0.882 | 0.895 |
| Kidney | 1 | 0.773 | 0.809 | 0.864 |
| | 2 | 0.786 | 0.798 | 0.839 |
| | 3 | 0.819 | 0.838 | 0.867 |
| | 4 | 0.808 | 0.818 | 0.851 |
| | 5 | 0.779 | 0.800 | 0.841 |
| | Mean | 0.793 | 0.813 | 0.852 |
| Liver | 1 | 0.802 | 0.838 | 0.863 |
| | 2 | 0.801 | 0.812 | 0.837 |
| | 3 | 0.809 | 0.824 | 0.862 |
| | 4 | 0.810 | 0.826 | 0.855 |
| | 5 | 0.812 | 0.816 | 0.860 |
| | Mean | 0.807 | 0.823 | 0.855 |

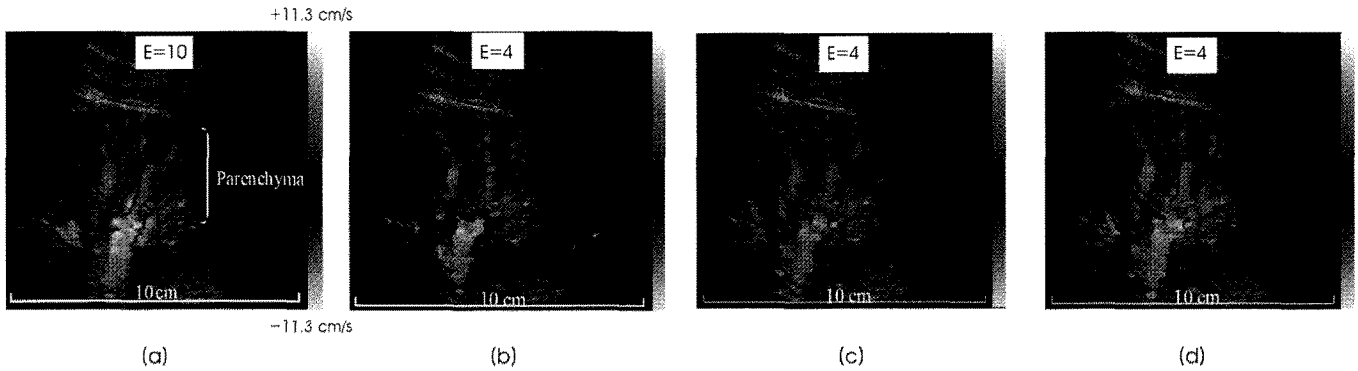


**Fig. 6.** Color Doppler images obtained from the kidney by applying (a) AC-ACR with E=10 as the reference, (b) AR, (c) ED, and (d) AC-ACR methods.

*AD*=-60 dB and *PG*=3.5. The ED and AC-ACR estimators provide higher sensitivity than the AR estimator when we compare Fig. 6(b)-6(d). Blood flow in the renal medulla and cortex is more clearly visualized in Fig. 6(c) and 6(d). In addition, the ED and AC-ACR estimators show more continuous arterial (red) and venous (blue) flow. These results are consistent with the ROC curves shown in Fig. 7. The ED and AC-ACR estimators provide higher sensitivity and specificity (i.e., higher *TP* and lower *FP*) compared to the AR method. Moreover, as listed in Table 2, the AC-ACR outperforms the ED in terms of AUC for E=4 (0.852 vs. 0.813, $p<0.01$).

The advantage of the ED and AC-ACR estimators over the AR estimator is more clearly demonstrated in Fig. 8 where the liver color Doppler images from Subject 1 are visualized when using *LS*=0.25 PRF and a window size of 3×3, *AD*=-60 dB and *PG*=3.5. Similar to the kidney case, the ED and AC-ACR estimators show improved sensitivity compared to the AR estimator. For example, the hepatic vein branches (red) in the liver parenchyma are more clearly shown in E=4. Furthermore, while the AR cannot visualize the flows in the inferior vena cava *(IVC)*, it is clearly depicted by the ED and AC-ACR estimators. The ROC curves for the liver data are shown in Fig. 9. The AC-ACR method outperforms the AR and ED estimators in terms of the sensitivity and specificity. This result is consistent with Table 2 where the AC-ACR provides higher AUC values compared to the ED and AR estimators for E=4 (i.e., 0.855 vs. 0.823 and 0.807, $p<0.01$).

### B. 3D *in vivo* data

Fig. 10 shows the color Doppler images with the velocity estimates obtained from a kidney transplant patient by applying AC-ACR for E=10 and E=4. The AC-ACR with E=10 in Fig. 10(a) is considered as the reference. Fig. 10(b) with E=4 shows comparable results upon visual examination against the reference. It successfully visualizes not only the iliac artery but also arcuate arteries in the renal parenchyma. The performance of AC-ACR with E=4 was quantified by

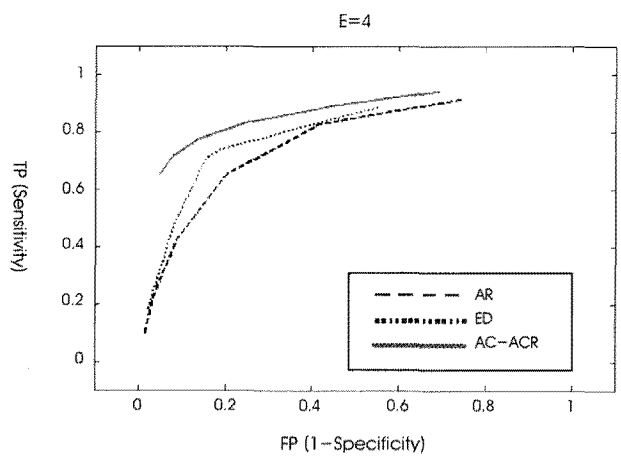


**Fig. 7.** ROC curves when applying the AR, ED and AC-ACR estimation methods to the 2D kidney data for E=4.

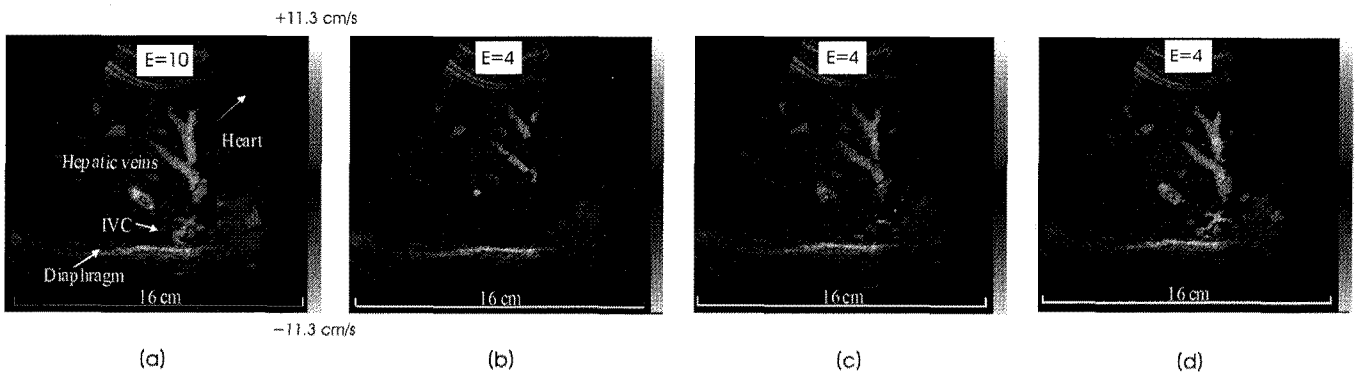


**Fig. 8.** Color Doppler images obtained from the liver by applying the (a) AC-ACR with E=10 as the reference, (b) AR, (c) ED, and (d) AC-ACR methods.

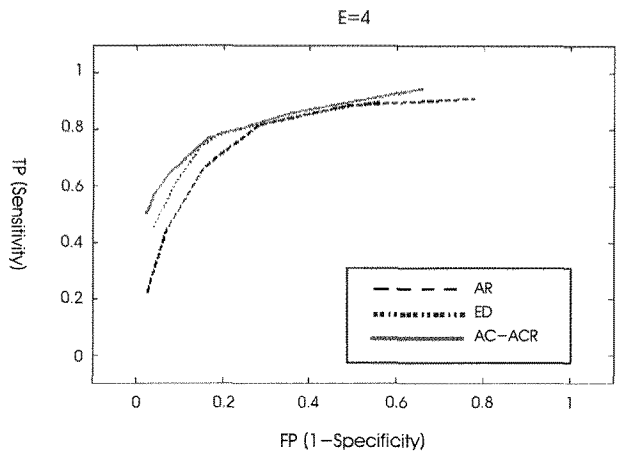


**Fig. 9.** ROC curves when applying the AR, ED, and AC-ACR estimators into the 2D liver data for E=4.

measuring AUC by changing the *PG* from 1.5 and 6.5, which led to the AUC value of 0.824.

The impact of lowered flow detection sensitivity with a smaller ensemble size was investigated by reconstructing the 3D vascular structures of the same patient's transplanted kidney as shown in Fig. 11 where two different views are shown. Compared to the reference rendered image (i.e., AC-ACR with E=10) in Fig. 11(a), Fig. 11(b) (E=4) shows comparable results in visualizing the vasculatures of the transplanted kidney. Although AC-ACR with a smaller ensemble size (E=4) lowers the sensitivity in flow detection (e.g., detecting arcuate arteries in the renal medulla and cortex), its impact on 3D vascular visualization is not perceivable as demonstrated in Fig. 11. In addition, it can successfully visualize the twisted renal artery in Fig. 11(b). AC-ACR with E=4 could double the volume acquisition rate

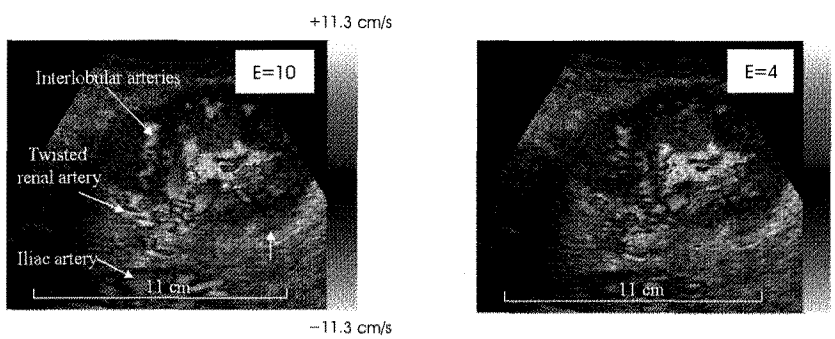


**Fig. 10.** Color Doppler images with the velocity estimates obtained from subject 1 by applying the AC-ACR method for (a) E=10 and (b) E=4.

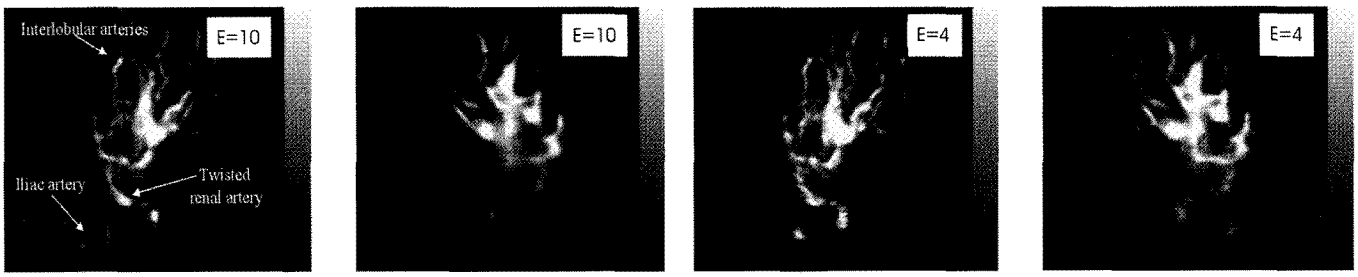


**Fig. 11.** Rendered color Doppler images with the power estimates obtained from the kidney transplant patient by applying the AC-ACR when (a) E=10 and (b) E=4 for two different viewing angles.

compared to the reference with E=10 for 3D CDI.

In summary, for the CCA case, the AR estimator outperforms the ED and AC-ACR estimators where the SNR and flow signal strength are higher than the kidney and liver cases. However, it suffers from the unwanted rejection of flow estimates due to aliasing. This aliasing can be avoided using a higher PRF, but the AR estimator would compromise its sensitivity to low velocity flow. In addition, its performance is degraded in case of the kidney and liver data. On the other hand, the ED estimator shows promising results in that it can reliably estimate flow velocities with small ensemble sizes. In the present study, only temporal samples in Eq. (2) were utilized to estimate the complex signal covariance matrix in Eq. (9), since it was not possible to access undecimated RF samples in the ultrasound machine we used. Using the RF samples together with the temporal samples, the robustness of the covariance matrix estimates could be improved. However, it will increase the computational complexity substantially due to a higher estimation order (p). The AC-ACR estimatior provides comparable results to the ED estimator. On the other hand, its computational requirement is much less than that of the ED estimator. Thus, AC-ACR would be more suitable for 3D CDI in order to improve the volume acquisition rate. Using AC-ACR with E=4, we can theoretically improve the volume acquisition rate by 2.5, compared to E=10.

## IV. CONCLUSION

To improve the temporal resolution in 3D CDI, an efficient flow estimation method that can provide robust estimates with a small number of pulse transmissions would be desired. In this paper, three flow estimation methods were evaluated using 2D and 3D *in vivo* data under different clutter conditions. From the 2D *in vivo* studies, the AC-ACR estimation method provides higher sensitivity with low variance in flow estimates compared to the AR method, while yielding similar specificity. In addition, it shows similar results compared to the ED estimator with a lower computational burden. Moreover, from the 3D *in vivo* study, AC-ACR with a smaller ensemble size shows its capability in visualizing the complex vascular morphology of the transplanted kidney. These results indicate that the AC-ACR estimation method could be useful for improving the volume acquisition rate in 3D CDI by reducing the number of pulse transmissions.

## ACKNOWLEDGEMENT

This work was partially supported by Industrial Source Technology Development Program (1003522, 10033702) funded by the Ministry of Knowledge Economy(MKE), Korea

## REFERENCES

[1] D.H. Pretorius, T. R. Nelson, and J. S. Jaffe, "3-dimensional sonographic analysis based on color flow Doppler and gray scale image data: a preliminary report," *J. Ultrasound Med.*, vol. 11, no. 5, pp. 225-232, 1992.

[2] R. D. Simone, G. Glombitza, C. F. Vahl, J. Albers, H. P. Meinzer, and S. Hagl, "Three-dimensional color Doppler: a new approach for quantitative assessment of mitral regurgitant jets," *J. Am. Soc. Echocardiogr.*, vo. 12, no. 3, pp. 173-185, 1999.

[3] U. Herberg, H. Goldberg, and J. Breuer, "Three- and four-dimensional freehand fetal echocardiography: a feasibility study using a hand-held Doppler probe for cardiac gating," *Ultrasound Obstet. Gynecol.*, vol. 25, no. 4, pp. 362-371, 2005.

[4] P. S. Mehwald, R. A. Rusk, Y. Mori, X. N. Li, A. D. Zetts, M. Jones, and D. J. Sahn, "A validation study of aortic stroke volume using dynamic 4-dimensional color Doppler: an *in vivo* study," *J. Am. Soc. Echocardiogr.*, vol. 15, no. 10, pp. 1045-1050, 2002.

[5] R. Chaoui, J. Hoffmann, and K. S. Heling, "Three-dimensional (3D) and 4D color Doppler fetal echocardiography using spatio-temporal image correlation (STIC)," *Ultrasound Obstet. Gynecol.*, vol. 23, no. 6, pp. 535-545, 2004.

[6] C. Kasai, K. Namekawa, A. Koyano, and R. Omoto, "Real-time

two-dimensional blood flow imaging using an autocorrelation techniques," *IEEE Trans. Sonics. Ultrason.*, vol. 32, no. 3, pp. 458-463, 1985.

[7] H. Tsujino, M. Jones, T. Shiota, J.X. Qin, L. A. Cardon, A. J. Morehead, A. D. Zetts, F. Bauer, M. Stiges, X. Hang, N. L. Greenberg, J. A. Panza, and J. D. Thomas, "Impact of temporal resolution on flow quantification by real-time 3D color Doppler echocardiography: numerical modeling and animal validation study," *Comput. Cardiol.*, vol. 27, pp. 761-764, 2000.

[8] J. Pemberton, L. Hui, M. Young, X. Li, A. Kenny, and D. J. Sahn, "Accuracy of 3-dimensional color Doppler-derived flow volumes with increasing image depth," *J. Ultrasound Med.*, vol. 24, no. 8, pp. 1109-1115, 2005.

[9] H. Torp, "Clutter rejection filters in color flow imaging: a theoretical approach," *IEEE Trans. Ultrason. Ferroelect. Freq. Control*, vol. 44, no. 2, pp. 417-424, 1997.

[10] S. Bjaerum, H. Torp, and K. Kristoffersen, "Clutter filters adapted to tissue motion in ultrasound color flow imaging," *IEEE Trans. Ultrason. Ferroelect. Freq. Control*, vol. 49, no. 6, pp. 693-704, 2002.

[11] Y. M. Yoo, R. Managuli, and Y. Kim, "An adaptive clutter filtering for ultrasound color flow imaging," *Ultrasound Med. Biol.*, vol. 29, no. 9, pp. 1311-1320, 2003.

[12] L.A.F. Ledoux, P.J. Brands and A.P.G. Hoeks, "Reduction of the clutter component in Doppler ultrasound signals based on singular value decomposition: a simulation study," *Ultrason. Imaging*, vol. 19, no. 1, pp. 1-18, 1997.

[13] D. E. Kruse and K. W. Ferrara, "A new high resolution color flow system using an eigendecomposition-based adaptive filter for clutter rejection," *IEEE Trans. Ultrason. Ferroelect. Freq. Control*, vol. 49, no. 12, pp. 1739-1754, 2002.

[14] T. Loupas and W. N. McDicken, "Low-order complex AR models for mean and maximum frequency estimation in the context of Doppler color flow mapping," *IEEE Trans. Ultrason. Ferroelect. Freq. Control*, vol. 37, no. 6, pp. 590-601, 1990.

[15] Y. B. Ahn and S. B. Park, "Estimation of mean frequency and variance of ultrasonic Doppler signal by using second-order autoregressive model," *IEEE Trans. Ultrason. Ferroelect. Freq. Control*, vol. 38, no. 3, pp. 172-182, 1991.

[16] M. E. Allam and J. F. Greenleaf, "Isomorphism between pulsed-wave Doppler ultrasound and direction-of-arrival estimation-part I: basic principles," *IEEE Trans. Ultrason. Ferroelect. Freq. Control*, vol. 43, no. 5, pp. 911-922, 1996.

[17] M. E. Allam, R. R. Kinnick, and J. F. Greenleaf, "Isomorphism between pulsed-wave Doppler ultrasound and direction-of -arrival estimation-part II: experimental results," *IEEE Trans. Ultrason. Ferroelect. Freq. Control*, vol. 43, no. 5, pp. 923-935, 1996.

[18] P. J. Vaitkus, and R. S. C. Cobbold, "A new time-domain narrowband velocity estimation technique for Doppler ultrasound flow imaging-part I: theory," *IEEE Trans. Ultrason. Ferroelect. Freq. Control*, vol. 45, no. 4, pp. 939-954, 1998.

[19] P. J. Vaitkus, R. S. C. Cobbold, and K. W. Johnston, "A new time-domain narrowband velocity estimation technique for Doppler ultrasound flow imaging-part II: comparative performance assessment," *IEEE Trans. Ultrason. Ferroelect. Freq. Control*, vol. 45, no. 4, pp. 955-971, 1998.

[20] Y. M. Yoo, S. Sikdar, K. Karadayi, O. Kolokythas, and Y. Kim, "Adaptive clutter rejection for 3D color Doppler imaging: preliminary clinical study," *Ultrasound Med. Biol.*, vol. 34, no. 8, pp. 121-1231, 2008.

[21] Marple SL. Digital Spectral Analysis with Applications. Prentice Hall, Englewood Cliffs, NJ, 1987.

[22] Stoica P, Moses R. Introduction to Spectral Analysis. Prentice Hall, Upper Saddle River, NJ, 1997.